Intermembrane docking reactions are regulated by membrane curvature

Supporting Information

Andreas H. Kunding, Michael W. Mortensen, Sune M. Christensen, Vikram K. Bhatia, Ivan Makarov, Ralf Metzler and Dimitrios Stamou

Materials

1,2-Dioleoyl-sn-Glycero-3-Phosphocholine (DOPC), 1,2-Dioleoyl-sn-Glycero-3-[Phospho-rac-(1-glycerol)] (Sodium Salt) (DOPG), 1,2-Dioleoyl-sn-Glycero-3-Phosphoethanolamine-N-(Cap Biotinyl) (Sodium Salt) (DOPE-biotin), L-α-Phosphatidylcholine (Brain, Porcine) (Brain PC), L-α-Phosphatidylserine (Brain, Porcine-Sodium Salt)(Brain PS), L-α-Phosphatidylinositol-4,5-bisphosphate (Brain, Porcine-Triammonium Salt) (PIP2), cholesterol (ovine wool)(>98%) and 1,2-Dioleoyl-sn-Glycero-3-Phosphoethanolamine-N-[Methoxy(Polyethylene-glycol)-2000] (Ammo-nium Salt) (DOPE-PEG_{2000}) were all purchased as chloroform solutions from Avanti Polar Lipids (Alabaster, AL, USA). Oregon Green 488 1,2-dihexadecanoyl-sn-glycero-3-phosphoethanolamine (DHPE-OrG_{488}), 1,1'-dioctadecyl-3,3,3',3'-tetramethylindo-carbocyanine perchlorate (DiI-C_{18}), 3,3'-dioctadecyloxacarbocyanine perchlorate (DiO-C_{18}) and 1,1'-dioctadecyl-3,3,3',3'-tetramethylindodicarbocyanine, 4-chlorobenzene-sulfonate salt (DiD-C_{18}) were also purchased as chloroform solutions from Invitrogen (Taastrup, Denmark). Poly(L-lysine)-g-poly(ethylene glycol)$_{45}$-(PLL-g-PEG_{2000}) and poly(L-lysine)-g-poly(ethylene glycol)$_{76}$-biotinyl (PLL-g-PEG_{3400})-biotin were purchased as solutions from Surface Solutions (Zürich, Schwitzerland). Octyl β-D-glucopyranoside (OGP), dithiothreitol (DTT), D-sorbitol, glycerol, 4-(2-hydroxyethyl)-1-piperazine-ethanesulfonic acid (HEPES), tris(hydroxymethyl)aminomethane (Tris) were all purchased as powder from Sigma-Aldrich (Brøndby, Denmark). Bio-Beads were purchased as powder from Bio-Rad Laboratories (Hercules, CA, USA). Detergent micelle solutions of rat neuronal syntaxin, SNAP-25 and synaptobrevin as well as solutions of wildtype synaptotagmin-1 C2AB domain were kind gifts from professor H. T. McMahon.

Syntaxin/SNAP-25-reconstitution in lipid vesicles. A thin lipid film was prepared as described in *Vesicle preparation*, see table S1 for lipid composition of vesicles. Lipids were hydrated by adding 50 mM Tris buffer (pH 8, 150 mM NaCl, 2 mM DTT) to a total lipid concentration of 10 mM. Lipids were incubated 15 min. and gently sonicated in a bath sonicator. The vesicles were extruded 3 times through a 0.8 µm filter using an Avanti mini-extruder. 10 µl vesicles were added to 90 µl 11.1 µM Syntaxin/SNAP25 heterodimer solution and allowed to incubate 15 min. at ambient temperature (A 1:1 Syntaxin:SNAP25 complex was formed just before use by incubating 5.3 µl 190 µM Syntaxin with 11.1 µl 90 µM SNAP25 1 hour at 4^{o}C. The complex concentration was adjusted to 11.1 µM using 50 mM Tris buffer (pH 8, 100 mM KCl, 10% Glycerol, 0.4% OGP, 5 mM DTT). The solution was diluted by adding 100 µl 50 mM Tris buffer (pH 8, 150 mM NaCl, 2 mM DTT). The detergents were removed by dialysis over night against 2 l 25 mM HEPES buffer (pH 7.5, 100 mM KCl, 5% glycerol, 2 mM DTT) and 10 g BioBeads at 4^{o}C.

Synaptobrevin-reconstitution in lipid vesicles. A thin lipid film was prepared as described in *Vesicle preparation*, see table S1 for lipid composition of vesicles. Lipids were hydrated by adding 50 mM Tris buffer (pH 8, 150 mM NaCl, 2 mM DTT) to a total lipid concentration of 10 mM. Lipids were incubated 15 min. and gently sonicated in a bath sonicator. The vesicles were extruded 21 times

through a 0.05 µm filter using an Avanti mini extruder. 20 µl vesicles were added to 80 µl 50 µM synaptobrevin solution and allowed to incubate 15 min. at ambient temperature (11.2 µl 358 µM synaptobrevin was diluted to 50 µM using 25 mM HEPES buffer (pH 7.5, 100 mM KCl, 10% Glycerol, 0.5% OGP, 4 mM DTT). The solution was diluted by adding 100 µl 50 mM Tris buffer (pH 8, 150 mM NaCl, 2 mM DTT). The detergents were removed by dialysis over night against 2 l 25 mM HEPES buffer (pH 7.5, 100 mM KCl, 5% glycerol, 2 mM DTT) and 10 g BioBeads at 4^{o}C.

Surface functionalization. Glass coverslips were sonicated in 2% (v/v) Hellmanex and in MilliQ water and stored in methanol. Prior to functionalization the coverslips were plasma-etched for two minutes in a PDC-32G plasma-cleaner (Harrick Plasma, New York, USA). To create polymer-passivated substrates we immediately after plasma-cleaning incubated the coverslips for 30 minutes with a mixture of PLL-PEG$_{2000}$ and PLL-PEG$_{2000}$-biotin in 10 mM HEPES buffer in the molar ratio 1000:1, respectively. Samples were washed 5 times with the HEPES buffer followed by 10 minutes of incubation with 0.025 g/l unlabeled neutravidin. Unbound neutravidin were removed by extensive washing. The functionalized glass-substrates were used immediately for experiments.

Supported lipid bilayer preparation. Glass coverslips were prepared as described above. Immediately after plasma-etching the glass coverslips were incubated with a 50-nm extruded SUV suspension (i.e. SUV$_{SLB}$, see table S1) at a nominal lipid concentration of 2.0 g/l. Samples were allowed to incubate for 40 minutes at 37 ^{o}C. Excess SUVs were removed by copious washing (> 50 times volume exchange) followed by incubation with 0.025 g/l NAv for 10 minutes. The samples were extensively washed with buffer to remove unbound NAv and used for experiments immediately. The integrity of the supported membranes were inspected with fluorescence photobleaching recovery and confirmed that the bilayers were in a fluid state.

Streptavidin-functionalization of lipid vesicles

Vesicles (SUV$_{200}$) were prepared as described in *Vesicle preparation* according to table S1 and diluted 100 times. Next a 10-fold molar excess of Oregon-Green488-labelled neutravidin (NAv) was added to the vesicle suspension. The SUVs were incubated for 2 hours at 4^{o}C. Excess NAv was subsequently removed by extensive dialysis at 4^{o}C (1 ml sample in 2 l buffer) for 24 hours and with 6 changes of buffer. The SUV sample was used immediately after preparation for docking experiments.

Dynamic light scattering

Experiments were performed using a multi-angle ALV-5000 compact goniometer system (Langen, Germany). SUV samples were diluted 10 times in the appropriate buffer system and light scattering at 633-nm were measured at several angles (70 ^{o}, 90 ^{o}, 110 ^{o}, 130 ^{o}, 150 ^{o}) and at a constant temperature of 21^{o}C. The average radius of SUV$_{50}$, extruded 15 times through a 50 nm filter, was found to be R_C = 28 ± 1 nm. For SUV$_{syb}$ we found R_C = 33 ± 3 nm. For SUV$_{200}$ we extracted the number-weighted size distribution *f(R)* from the correlation-function using the dls 2g(t) regularized fit routine implemented in the ALV correlator software. The formfactor of vesicles with a membrane thickness of 4 nm was applied.

Image analysis

Recorded micrographs were quantified using custom software programmed in Igor Pro v.6 (Wavemetrics, Oregon, USA). The position of SUVs was identified from the micrographs by setting an

intensity threshold to localize pixel-assemblies greater than a specified minimum area and with intensity-values above the threshold. SUV intensities were extracted by applying a 2D-Gaussian fit to the intensity distribution and calculating the integrated (background corrected) signal. For each Gaussian fit we additionally extracted the skewness of the 2D intensity distribution (Eqn. S1), i.e. the elliptical major and minor axis and tilt angle. For each frame we recorded all SUV positions and compared them to the subsequent frame, thus enabling tracking and classification of particles(1). We considered a SUV as docked, when the center position did not change >5 pixels/frame. Otherwise we classified the SUV as diffusing.

Measurement of the microscope point spread function

The point spread function (PSF) of the confocal laser scanning microscope was measured by acquiring images of the glass/buffer interface of a microscope glass-slide with buffer deposited on it. Contrast on the image was generated by monitoring the scattered light intensity originating from the glass/buffer interface. The interface can be considered as a point-like scatterer and we thus obtained the PSF directly from a line intensity profile of the micrograph. We subtracted background intensity and normalized the PSF to 1.0 at maximum, thus yielding the detection efficiency profile $p(z, \lambda)$.

Determination of SUV radius from fluorescence intensity

We determined the radius of individual SUVs by measuring their fluorescence intensity signal from micrographs. The procedure is described in more detail in reference (2). Briefly, we applied a global threshold-intensity (T_I) to all micrographs to identify pixel-assemblies exhibiting a higher pixel-wise intensity. To eliminate noise we only accepted collections of pixels greater than a certain minimum-area (A_M). Both T_I and A_M were consistently held constant for micrographs acquired with the same microscope settings. Next, we extracted the total SUV intensity signal (I_T) from a 2D-Gaussian fit to the part of the micrograph containing the SUV:

$$I(x,y) = I_{BG} + A\exp\left(-\frac{x_R^2}{w_x^2} - \frac{y_R^2}{w_y^2}\right) \qquad \text{Eqn. S1}$$

Here, I_{BG} is the background intensity, A is the intensity amplitude, w_x and w_y are the widths along the x- and y-axis, respectively. x_R and y_R are rotated coordinates to allow for arbitrary orientation of the Gaussian function:

$$\begin{aligned} x_R &= (x - x_0)\cos\theta - (y - y_0)\sin\theta \\ y_R &= -(x - x_0)\sin\theta - (y - y_0)\cos\theta \end{aligned} \qquad \text{Eqn. S2}$$

Here, x_0 and y_0 constitutes the center-position of the SUV and θ is the tilt angle about the x-axis. Next, we converted I_T to radius applying the following relation:

$$I_T(R) = \frac{I_0}{\int_{z=0}^{2R_0} p(z,\lambda)G(R_0,z)dz} \int_{z=0}^{2R} p(z,\lambda)G(R,z)dz \qquad \text{Eqn. S3}$$

Here, $p(z, \lambda)$ is the normalized point spread function (PSF) of the microscope along the optical-axis, R_0 is the average radius obtained from a dynamic light scattering measurement on the SUV_{50}-population, see table S1. I_0 is the corresponding average intensity of the SUV_{50}-sample obtained from particle analysis of fluorescence micrographs. $G(R, z)$ is a geometric function describing the object, in this case we assume SUVs to be spherical shells, thus $G(R,z) = 2\pi\sqrt{2Rz - z^2}$. Approximating $p(z, \lambda)$ to a 1D Gaussian function with width w_z, we can rewrite Eqn. S3 to

$$I_T(R) = I_0 \frac{R}{R_0} \frac{\mathrm{erf}\left(2R/w_z\right)}{\mathrm{erf}\left(2R_0/w_z\right)} \qquad \text{Eqn. S4}$$

We thus extracted R-values directly from the total intensity by constructing an intensity look-up table applying Eqn. S4.

Determination of NAv membrane densities

We determined the membrane-density of NAv bound to either an SLB or a SUV as described in reference (3). Briefly, we acquired fluorescence micrographs of a calibration sample consisting of a NAv-solution with known concentration (C_0). From the micrographs we measured (and background-corrected) the average pixel intensity (I_0). Next, we measured the pixel fluorescence intensity (I) from NAv bound to an SLB and converted this value to surface density (σ) according to

$$\sigma = \frac{I}{I_0} \frac{\sqrt{\pi} C_0 w_z}{2} \qquad \text{Eqn. S5}$$

For the case of NAv bound to the membrane of SUVs we modified Eqn. S5, so it could be applied to a sub-resolution spherical shell geometry:

$$\sigma = \frac{I_T}{2I_0} \frac{A_P C_0}{\mathrm{R} \cdot \mathrm{e}\, rf\left(\frac{2R}{w_z}\right)} \qquad \text{Eqn. S6}$$

Here, I_T is the total (and background-corrected) fluorescence intensity from NAv bound to a SUV of radius R. A_P is the apparent pixel area, i.e. micrograph area divided by number of pixels. For measured membrane densities of NAv, see table S3.

Calculation of N_{DIF} for a SLB

To calculate N_{DIF} for a SLB we apply the following result from reference (4): For a particle with diffusion coefficient D situated in a one-dimensional box of length a, the mean time to capture (τ), i.e. the time before the particle hits the right-hand wall, equals $\tau = a^2/3D$. This results assumes that only one boundary in the box can bind the particle, whereas the other boundary reflects it. We now consider a cubic box of volume a^3 having a single absorbing surface. The mean time to capture remains the same, because only diffusion along the normal to the absorbing surface contributes to τ, thus the

diffusive flux (J) onto the absorbing surface equals

$$J = \frac{1}{a^2 \tau} = \frac{3D}{a^4} = 3DC_V^{4/3} \qquad \text{Eqn. S7}$$

Here, we made use of the fact that the volume available to a single particle is inversely proportional to its concentration, i.e. $a^3 = 1/C_V$. A SLB with area A_{SLB} will then experience the following number of docking attempts during the time-duration t:

$$N_{DIF} = JA_{SLB}t = 3DA_{SLB}C_V^{4/3}t \qquad \text{Eqn. S8}$$

Measurement of L_z, L_{xy} and t_P

A SUV is considered detectable if it exhibits an E_C-value greater than E_{CT}. E_C is a function of the distance d the particle moves during the acquisition time t_P. We consider a SUV detectable if it remains inside a (detection)-box of length L_z along the optical axis (z-axis) and length L_{xy} in the lateral plane. If the particle ventured outside the box it would appear more elongated, than allowed for by the E_{CT}-value, see Fig. 2B-C.

L_z corresponds to the maximum distance above the focus-plane a particle is still distinguishable from the background- and noise-signals. Assuming the particle to attain a 2D-Gaussian intensity distribution (Eqn. S1) on the micrograph, we can calculate L_z directly from the Gaussian parameters and the PSF along the optical axis:

$$L_z = w_z \sqrt{\ln\left(\frac{A}{T_I - I_{BG}}\right) - \frac{A_M}{\pi w_x w_y}} \qquad \text{Eqn. S9}$$

Here, A, I_{BG}, w_x, w_y are 2D-Gaussian parameters, w_z is the width of the PSF, T_I and A_M are threshold intensity and minimum particle area, respectively. Both T_I and A_M are user-specified parameters set during particle analysis to identify particles from a micrograph.

Analogously, we can calculate the time it takes for the confocal microscope to scan a particle. The time is obtained by dividing the number of pixel-lines (N_{PL}) constituting the particle along the scan-direction (x-axis) with the scan-speed (v):

$$t_P = \frac{N_{PL}}{v} = \frac{2w_x}{v} \sqrt{\ln\left(\frac{A}{T_I - I_{BG}}\right)} \qquad \text{Eqn. S10}$$

L_{xy} was numerically evaluated based on the eccentricity-threshold (E_{CT}) applied to analyze the diffusing SUVs. This was achieved by creating an artificial micrograph of a single particle from the 2D-Gaussian parameters obtained from the immobilized SUV sample. Next, we created another artificial micrograph, where the center of the particle had been displaced a distance d. We then added the two micrographs and fitted Eqn. S1 to the resulting intensity distribution, thus obtaining E_C as a function of

d. In this way we constructed a look-up table of corresponding *d*- and E_C-values, see Fig. S1A. L_{xy} is obtained from this table by reading off the *d*-value at the eccentricity-threshold, i.e. $L_{xy} = d\left(E_{CT}\right)$.

Derivation of the fraction of detected diffusing SUVs

We will here derive an expression for the fraction (F_D) of diffusing SUVs that are detectable in an experiment. To calculate F_D we consider the one-dimensional case, where a particle is situated at $x = a < L_x$ in a box ranging from $x = 0$ to $x = L_x$. From Einstein's distribution of particle displacements during diffusion (5), we get the chance *f* that the particle will remain inside the box during the time t_P is

$$f(a) = \frac{1}{2}\left(\operatorname{erf}\left(\frac{a}{\sqrt{4Dt_P}}\right) - \operatorname{erf}\left(\frac{L_x - a}{\sqrt{4Dt_P}}\right)\right) \qquad \text{Eqn. S11}$$

We can calculate the detected fraction along the *x*-axis by averaging *f(a)* over the entire box-length, i.e. $a = 0$ to L_x:

$$F_D^x = \frac{1}{L_x}\int_{a=0}^{l} f(d)\,da = \operatorname{erf}\left(\frac{L_x}{\sqrt{4Dt_P}}\right) + \frac{L_x}{\sqrt{4\pi Dt_P}}\left(\exp\left(-\frac{L_X^2}{4Dt_P}\right) - 1\right) \qquad \text{Eqn. S12}$$

The calculation along the *y*-axis is identical, whereas the *z*-axis has incorporated a reflective boundary at $z = 0$ corresponding to the surface of the glass-substrate in the experiment. The total detected fraction is found by multiplication of the three one-dimensional cases, thus leading to

$$F_D = \left(\operatorname{erf}\left(\alpha_{xy}\right) + \frac{\exp\left(-\alpha_{xy}^2\right) - 1}{\alpha_{xy}\sqrt{\pi}}\right)^2 \times \left(\operatorname{erf}\left(2\alpha_z\right) + \frac{\exp\left(-4\alpha_z^2\right) - 1}{2\alpha_z\sqrt{\pi}}\right) \qquad \text{Eqn. S13}$$

Derivation of the bond formation probability

Assuming the formation of a single receptor/ligand-complex to be independent of all other complexes formed, i.e. each complex is formed with equal probability $P_{R,L}$, then we can apply the binomial distribution to calculate the chance (*P(N)*) to form exactly *N* bonds within the contact-area upon contact:

$$P(N) = \frac{1}{2}\left[\frac{N_L!}{N!\left(N_L - N\right)!}P_R^N\left(1 - P_R\right)^{N_L - N} + \frac{N_R!}{N!\left(N_R - N\right)!}P_L^N\left(1 - P_L\right)^{N_R - N}\right] \qquad \text{Eqn. S14}$$

The probability to form at least N_0 bonds (P_B) is thus

$$P_B = 1 - \sum_{N=0}^{N_0 - 1} P(N) \qquad \text{Eqn. S15}$$

To obtain a more straightforward expression for P_B we approximate the discrete binomial distribution with the continuous Gaussian function centered at $x_{R,L} = N_{R,L}P_{L,R} = A_C\rho_R\rho_L A_{CS}$ and with a standard deviation of $\sigma_{R,L} = \sqrt{x_{R,L}\left(1-\rho_{L,R}A_{CS}\right)}$. We can thus replace the sum in Eqn. S15 with an integral:

$$P_B = 1 - \frac{1}{2}\int_{N=0}^{N_0}\left[\frac{1}{A_R\sqrt{2\pi}\sigma_R}\exp\left(-\frac{\left(N-x_R\right)^2}{2\sigma_R^2}\right) - \frac{1}{A_L\sqrt{2\pi}\sigma_L}\exp\left(-\frac{\left(N-x_L\right)^2}{2\sigma_L^2}\right)\right]dN \qquad \text{Eqn. S16}$$

Here, A_R and A_L are normalization factors that compensate for the fact that the binomial distribution only is defined for $N \geq 0$, whereas the Gaussian distribution is defined for both positive and negative values of *N*. The normalization is given as

$$A_{R,L} = \int_{N=0}^{\infty}\frac{1}{\sqrt{2\pi}\sigma_{R,L}}\exp\left(-\frac{\left(N-x_{R,L}\right)^2}{2\sigma_{R,L}^2}\right)dN \qquad \text{Eqn. S17}$$

In most cases $A_{R,L} \sim 1$. Solving Eqn. S16 yields

$$P_B = 1 - \frac{1}{2}\left[\frac{\operatorname{erf}\left(\frac{N_0-x_R}{\sqrt{2}\sigma_R}\right) - \operatorname{erf}\left(-\frac{x_R}{\sqrt{2}\sigma_R}\right)}{1-\operatorname{erf}\left(-\frac{x_R}{\sqrt{2}\sigma_R}\right)} + \frac{\operatorname{erf}\left(\frac{N_0-x_L}{\sqrt{2}\sigma_L}\right) - \operatorname{erf}\left(-\frac{x_L}{\sqrt{2}\sigma_L}\right)}{1-\operatorname{erf}\left(-\frac{x_L}{\sqrt{2}\sigma_L}\right)}\right] \qquad \text{Eqn. S18}$$

Supporting References

1. Anthony, S. M., L. Hong, M. Kim, and S. Granick. 2006. Single-particle colloid tracking in four dimensions. Langmuir 22:9812-9815.
2. Kunding, A. H., M. W. Mortensen, S. M. Christensen, and D. Stamou. 2008. A fluorescence-based technique to construct size distributions from single-object measurements: application to the extrusion of lipid vesicles. Biophys. J. 95:1176-1188.
3. Bhatia, V. K., K. L. Madsen, P. Y. Bolinger, A. Kunding, P. Hedegard, U. Gether, and D. Stamou. 2009. Amphipathic motifs in BAR domains are essential for membrane curvature sensing. EMBO J. 28:3303-3314.
4. Berg, H. C. 1983. Random walks in biology. Princeton University Press. 17-47.
5. Einstein, A. 1905. Über die von der molekularkinetischen Theorie der Wärme geforderte Bewegung von in ruhenden Flüssigkeiten suspendierten Teilchen. Ann. Phys. 17:549-560.
6. LeNeveu, D. M., and R. P. Rand. 1977. Measurement and modification of forces between lecithin bilayers. Biophys. J. 18:209-230.
7. Gandhavadi, M., D. Allende, A. Vidal, S. A. Simon, and T. J. McIntosh. 2002. Structure, composition, and peptide binding properties of detergent soluble bilayers and detergent resistant rafts. Biophys. J. 82:1469-1482.
8. Marra, J. 1986. Direct Measurements of Attractive van der Waals and Adhesion Forces between Uncharged Lipid Bilayers in Aqueous-Solutions. J Colloid Interface Sci 109:11-20.
9. Marra, J., and J. Israelachvili. 1985. Direct measurements of forces between phosphatidylcholine and phosphatidylethanolamine bilayers in aqueous electrolyte solutions. Biochemistry 24:4608-4618.
10. Martens, S., M. M. Kozlov, and H. T. McMahon. 2007. How synaptotagmin promotes membrane fusion. Science 316:1205-1208.
11. Grabner, C. P., S. D. Price, A. Lysakowski, and A. P. Fox. 2005. Mouse chromaffin cells have two populations of dense core vesicles. J. Neurophysiol. 94:2093-2104.

Table S1

	SUV^{*}_{SLB}	**SUV_{SLB}**	**SUV^{*}_{200}**	**SUV_{200}**	**SUV_{50}**
DOPC	89.5 mol%	90.0 mol%	57.7 mol%	59.7 mol%	87.7 mol%
DOPG			30.0 mol%	30.0 mol%	8.0/ 0.0 mol%
DOPE-biotin	10.0 mol%	10.0 mol%	10.0 mol%	10.0 mol%	2.0/10.0 mol%
DOPE-PEG_{2000}			0.3 mol%	0.3 mol%	0.3 mol%
DHPE-OrG_{488}	0.5 mol%				
DiD-C18			2.0 mol%		2.0 mol%
Extrusion filter	50 nm	50 nm	200 nm	200 nm	50 nm

Table S1: Lipid composition of vesicles applied in NAv/biotin-mediated docking-experiments. SUV^{*}_{SLB} was applied to the production of SLBs, whereas SUV_{SLB} was applied in surface-density calibration experiments to form SLBs displaying fluorescence-labelled neutravidin. SUV^{*}_{200} was applied both as the diffusing vesicle population in SUV/SLB-docking experiments (Fig. 5A), but also as the immobilized population in SUV/SUV-docking experiments (Fig. 5C). SUV_{200} was used for dynamic light scattering measurements. SUV_{50} was applied as the diffusing vesicle population in SUV/SUV-docking experiments (Fig. 5C) as well as a calibration sample to determine SUV radii. All vesicles were prepared in 10 mM phosphate buffered saline, pH 7.4, 80/120 mM NaCl. The osmolarity was adjusted with D-sorbitol.

Table S2

	$SUV_{syx/SNAP-25}$	**SUV_{syb}**
Brain-PC	57.9 mol%	73.0 mol%
Brain-PS	25.0 mol%	15.0 mol%
Cholesterol	10.0 mol%	10.0 mol%
PIP_2	5.0 mol%	
DOPE-biotin	0.1 mol%	
DiI-C18	2.0 mol%	
DiO-C18		2.0 mol%

Table S2: Lipid composition of vesicles applied in SNARE/syt-mediated docking-experiments. $SUV_{syx/SNAP-25}$ was applied as reconstitution vessels for syntaxin and SNAP-25. SUV_{syb} was applied for reconstitution of synaptobrevin.

Table S3

Docking type	**SUV/SLB**	**SUV/SLB**	**SUV/SUV**	**SUV/SUV**
Tethers	NAv/biotin	NAv/biotin	NAv/biotin	SNARE/syt
R_C (nm)	∞	∞	28	33
κ (m^{-1})[*]	$1.14 \cdot 10^9$	$0.93 \cdot 10^9$	$1.14 \cdot 10^9$	$1.14 \cdot 10^9$
B (Pa)[†]	10^{10}	10^{10}	10^{10}	10^{10}
λ_H (nm)[†]	0.193	0.193	0.193	0.193
t (nm)[‡]	3.6	3.6	3.6	3.6
A_0 (J)[§]	$3.5 \cdot 10^{-21}$	$3.5 \cdot 10^{-21}$	$3.5 \cdot 10^{-21}$	$3.5 \cdot 10^{-21}$
A_1 (J)[§]	$3.5 \cdot 10^{-21}$	$3.5 \cdot 10^{-21}$	$3.5 \cdot 10^{-21}$	$3.5 \cdot 10^{-21}$
Ψ(mV)	187 [¶]	228 [¶]	187 [¶]	85 [‖]
Ψ_C (mV)	47 [¶]	57 [¶]	47 [¶]	199 [‖]
ρ_R (10^{16} m^{-2})	1.19 [**]	1.19 [**]	$0.7 + 1.8 \cdot \exp(-0.046 \cdot R)$ [**]	$3.3 \cdot \exp(-0.012 \cdot R)$ [††]
ρ_L (10^{16} m^{-2})[‡‡]	15.6	15.6	3.13	1.56

Table S3: Parameters applied during the fitting of docking efficiency profiles shown in Fig. 5A, (column 1 and 2), Fig. 5C (column 3) and Fig. 5E (column 4).

[*] Inverse Debye screening length based on [Na^+] = 120 mM (first and third column), [Na^+] = 80 mM (second column) and [Na^+ + Ka^+] = 120 mM (fourth column).

[†] Values obtained for lecithin bilayers in reference (6)

[‡] Value obtained for a fluid phase DOPC bilayer in reference (7)

[§] Values obtained for various lipid bilayers in references (8, 9)

[¶] Surface potentials calculated based on the amount of charged lipids in the membrane. We have here considered only DOPG and DOPE-biotin, which both carries one negative charge.

[‖] Surface potentials calculated based on the amount of charged lipids in the membrane. We have here considered only brain PS and DOPE-biotin, which both carries one negative charge and PIP_2, which carries two negative charges.

[**] Values for the membrane density of NAv were measured as described above. It has been taken into account that one NAv-molecule on average display 2 binding-sites available for docking. R is measured in units of nm.

[††] Expression obtained from the membrane-density of synaptotagmin-1 (syt) in reference (10) and the reconstitution density of synaptobrevin (syb) (1 protein to 50 lipids corresponding to a syb-density of $3.3 \cdot 10^{16}$ m^{-2}), see Fig. S1B. In reference (10) relative densities of syt were measured for various SUV sizes. From this we obtained a relative density-decay constant of 0.012 nm^{-1}, see Fig. S1B inset. Assuming that a docking-competent complex consists of both syb and syt in a 1:1 ratio, we normalized the relative syt-density to the membrane-density of syb, i.e. $\rho_R(R) = 3.3 \cdot 10^{16} \exp\left(-0.012 \cdot R\right)$ m^{-2}.

[‡‡] Columns 1-3 displays the membrane-density of biotin calculated from the SUV lipid composition in table S1. Column 4 displays the membrane-density of the hetero-dimer syntaxin/SNAP-25 calculated from the protein-to-lipid ratio of 1:200.

Supporting legends

Fig. S1: **(A)** Eccentricity-values as a function of displacement calculated with A = 141, w_x = 2.01 and w_y = 1.90 representing population averages as obtained from the SUV_{50}-calibration experiment in (A). The threshold at E_{CT} = 0.75 corresponds to a displacement of d = 2.15 pixels, i.e. L_{xy} = 189.0 nm. Error-bars are the standard deviation of the measured E_C-value resulting from displacing the particle isotropically along 8 different directions. **(B)** Membrane density of synaptobrevin/synaptotagmin-1 (syb/syt) on surface-immobilized SUVs (SUV_{syb}, table S2). For further details see table S3. Inset shows an exponential fit to data on synaptotagmin-1 from reference (10).

Fig. S2: Efficiency of exocytosis obtained from inspection of combined electrophysiological and electron microscopic data of reference (11). **(A)** Size distribution of dense core vesicles in mouse chromaffin cells reproduced from Fig. 4A in reference (11). **(B)** Distribution of number of exocytic events as a function of quantal size ~ vesicle size reproduced from Fig. 4B in reference (11). **(C)** Exoctytic efficiency profile obtained by dividing the quantal size distribution in (B) with the vesicle size distribution in (A), i.e. fusion events per available vesicle. The profile was fitted to an exponential decay (black line). Inset shows a zoom-in on the first part of the graph without including the first point.

Figure S1

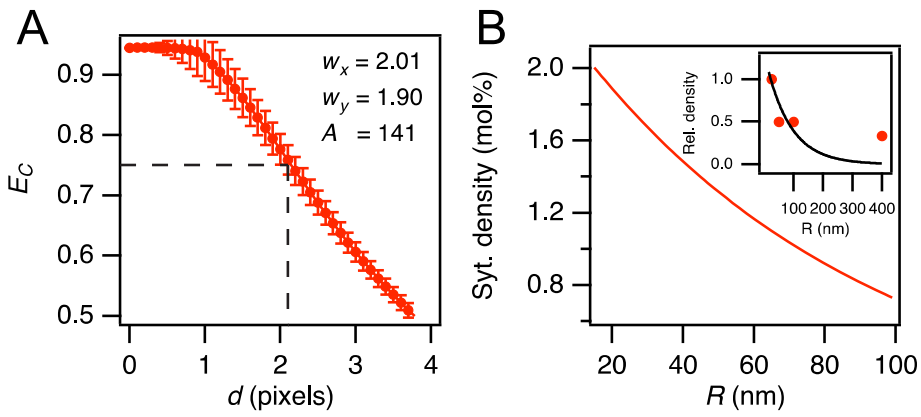
A
B
w_x = 2.01
w_y = 1.90
A = 141
E_C
d (pixels)
Syt. density (mol%)
R (nm)
Rel. density
R (nm)

Figure S2

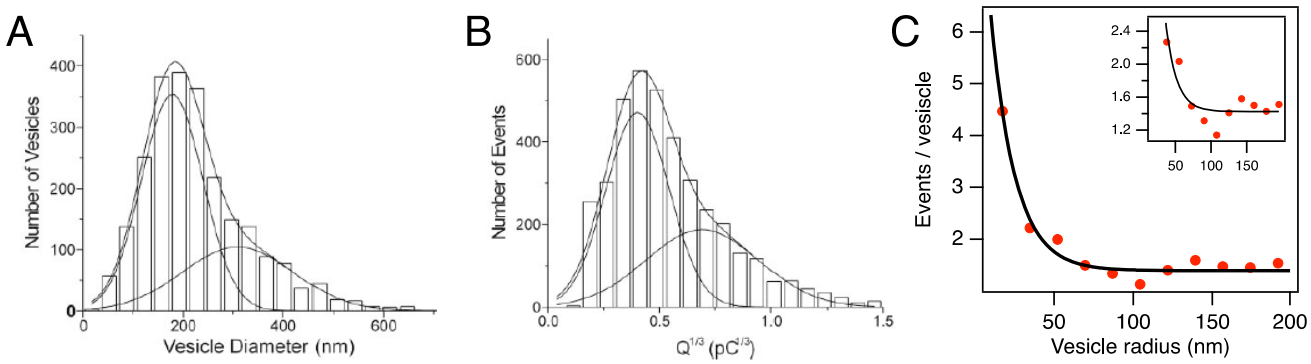
A
Number of Vesicles
Vesicle Diameter (nm)
B
Number of Events
$Q^{1/3}$ ($pC^{1/3}$)
C
Events / vesiscle
Vesicle radius (nm)